ORIGINAL PAPER

Multi-scale Experimental Investigations on the Deterioration Mechanism of Sandstone Under Wetting–Drying Cycles

Chong Wang[1,2] · Wansheng Pei[1,2] · Mingyi Zhang[1,2] · Yuanming Lai[1,2] · Jinpeng Dai[3]

Abstract

The repeated wetting–drying (WD) cycles can cause the deterioration of rock and thus affect the service performance of the related rock engineering, e.g., the crushed-rock embankment and the reservoir. The study comprehensively investigated the deterioration mechanism of sandstone under the WD cycles based on a series of multi-scale experiments, including the microstructure, the meso–micro pore characteristics, and the macroscopic physical and mechanical properties. The results indicate that the content of dissolved minerals and the permeability are two key factors that determine the deterioration effect caused by the WD cycles. During the WD cycles, the pore size range of sandstone becomes wider due to the formation of new small pores and the connection of original pores. Thus, low-density area forms within the samples, which causes the increasing of density dispersion. The structure deterioration weakens the physical and mechanical properties of the samples. The ultrasonic test indicates that the decreasing rate of the P-wave velocity is larger than that of the S-wave velocity, especially in the first 5 cycles. Besides, the exponential equations of uniaxial compressive strength and elastic modulus with the number of WD cycles are established to describe the deterioration of mechanical characteristics.

1 Introduction

Rock is a common material in engineering, e.g., the crushed-rock embankment (Lai et al. 2009; Pei et al. 2017; Tai et al. 2020), the rock slope (Xu and Yang 2018; Zheng et al. 2019; Song et al. 2018; Yang and Yin 2010), the rock foundation (Yang and Yin 2005; Chen and Ai 2020; Tang and Liu 2012), and the tunnel surrounding rock (Yang and Huang 2011; Shi et al. 2019; Lv et al. 2019). Rock in these constructions suffers long-term wetting–drying (WD) cycles due to the rainfall and evaporation, and water-level fluctuation. WD cycles can cause the performance deterioration of the rock due to the water–rock interaction (Yao et al. 2011; Pardini et al. 1996). Thus, it is a key factor that affects the

service performance of rock engineering. Numerous investigations have been conducted to study the deterioration mechanism of rock under WD cycles (Yao et al. 2011,2020; Pardini et al. 1996; Hua et al. 2017; Liu et al. 2016a, 2018a; Zhao et al. 2017; Cai et al. 2020; Yang et al. 2019; Qin et al. 2018; Torres-Suarez et al. 2014).

Currently, the experimental investigations of rock deterioration can be divided into three categories: macro-scale, meso-scale, and micro-scale. In macro-scale, the existing literatures mainly focus on the physical and mechanical properties (Yao et al. 2011; Pardini et al. 1996; Hua et al. 2015, 2017; Liu et al. 2016a, 2018a; Zhao et al. 2017,2018; Hale and Shakoor 2003; Dehestani et al. 2020; Song et al. 2019; Xie et al. 2019; Khanlari and Abdilor 2015; Zhou et al. 2017; Zhang et al. 2014; Özbek 2014). Pardini et al. (1996) found that the bulk density of mudrock decreased slightly and the porosity increases with the increasing number of WD cycles. Hua et al. (2015) indicated both the mode I fracture toughness and tensile strength of sandstone decreased with increase of the number of WD cycles. Zhao et al. (2017) concluded that the effect of WD cycles on the tensile strength of sandstone depended on the clay mineral content. Arash Dehestani et al. (2020) obtained the influence law of WD cycles on fracture

✉ Wansheng Pei
peiwansheng@lzb.ac.cn

1 State Key Laboratory of Frozen Soil Engineering, Northwest Institute of Eco-Environment and Resources, Chinese Academy of Sciences, Lanzhou 730000, China

2 University of Chinese Academy of Sciences, Beijing 100049, China

3 Lanzhou Jiaotong University, Lanzhou 730070, China

toughness and porosity. Khanlari and Abdilor (2015) statistically obtained the deterioration ratio of the physical and mechanical properties (P-wave velocity, porosity, and UCS) of red sandstone under the WD cycles. Özbek (2014) showed that the greatest change in uniaxial compressive strength (UCS) for black ignimbrites after 50 WD cycles can reach -16.08%. However, Hale and Shakoor (2003) found that the WD cycles had no significant effect on the unconfined compressive strength of the studied sandstone.

To further explore the mechanism of macroscopic deterioration, researchers recently carried out series of microscopic tests using the scanning electron microscope (SEM) (Hua et al. 2017; Liu et al. 2018a; Xie et al. 2019; Zhou et al. 2012, 2017; Zhang et al. 2014,2018; Zhao et al. 2018). Zhou et al. (2017) observed that the growth and expansion of microcracks after WD cycles can result in reduction of dynamic compressive strength of sandstone. Liu et al. (2018a) investigated that three stages sequently occurred for the microstructure of shaly sandstone under the WD cycles, including the well-organized dense structure stage, the porous stage, and the cracking stage. Zhang et al. (2014) found that WD cycles can cause argillization phenomenon in sandstone, and thus weaken the cement between sandstone particles.

The mesoscopic variation is a key perspective to reasonably connect the microscopic structure change and macroscopic phenomenon. With the application of computed tomography (CT) scan technique and the nuclear magnetic resonance (NMR) technique in geomaterials, many mesoscopic studies have also been conducted (Shen et al. 2020; Liu et al. 2019; Wang et al. 2014; Takano et al. 2015; Sun et al. 2020; Li et al. 2016,2018; de Argandoña et al. 1999; Zhang et al. 2004,2019a). Zhao et al. (2018) tested the influence of WD cycles on the pore structure of mudstone samples. Based on the test of pore structure by NMR technology, Shen et al. (2020) provided a practicable evaluation method on the influence of freeze–thaw on fracture rock mass and corresponding interface damage mechanism based on the NMR technique. Liu et al. (2016a) established the variation rate functions of damage taking the mean CT number as the damage variable.

The above studies have revealed the variations of rock under WD cycles from several scales. Although those studies can provide theoretical basis and guidance for practical engineering, few literatures can effectively analyze the damage mechanism of rock under the WD cycles by combining the macro, meso, and micro scales. The damage of materials starts from micro-scale and expands to other scales (Torres-Suarez et al. 2014; Zhou et al. 2016). Different processes occur at different scales, and these phenomena are actually interrelated. Consequently, to systematically explore the effect of WD cycles on the deterioration mechanism of rock, we conducted series of multi-scale investigations in this study. By comprehensively considering the response processes at different scales, we evaluated the deterioration characteristics of sandstone under WD cycles.

2 Materials and Methods

2.1 Sandstone Characteristics

Rock samples used in the test are sandstone. All samples are from the same rock mass with good homogeneity. Mineral composition was tested by the D8 advance X-ray diffraction system. The energy spectrum analysis results of the samples in initial state indicate that the sandstone is mainly composed of quartz (57.2%), calcite (19.7%), and albite (23.1%) (Fig. 1).
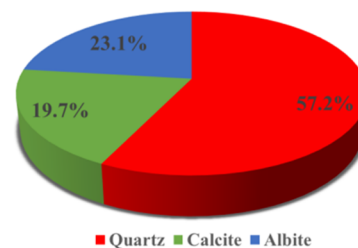
The initial physical and mechanical properties of sandstone without WD cycles are shown in Table 1.

2.2 Samples Preparation and Test Scheme

According to the International Society of Rock Mechanics (ISRM) test procedures (Khanlari and Abdilor 2015; Zhang et al. 2018; Lu et al. 2019), samples were cored from the rock mass and processed into cylinders with the diameter of 50 mm and the height of 100 mm. To eliminate the effect of size and initial structure difference, samples that do not meet the specifications (Table 2) were removed.
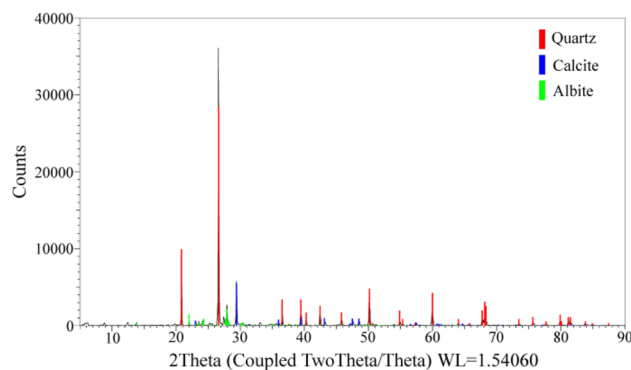
(a) Diagram of the X-ray analysis

(b) Mineral composition proportion

Fig. 1 Energy spectrum analysis results of sandstone without WD cycles

Table 1 Physical and mechanical properties of sandstone

Dry density (g/cm^3)	P-wave velocity (m/s)	S-wave velocity (m/s)	Porosity (%)	UCS (MPa)
2.41	3372.46	2278.62	2.239	76.35

All sandstone samples were divided into 6 groups, and samples in each group experienced 0, 3, 5, 10, 15, and 20 WD cycles, respectively. To enhance the reliability of experimental results, each group has 6 samples (Fig. 2). For each cycle, samples were firstly put into the vacuum saturator to absorb water for 24 h, and then dried in an oven at 105 ℃ for 24 h.

3 Experimental Results and Discussion

3.1 Analysis of Microstructure Changes

In order to intuitively study the changes of microstructure caused by WD cycles, SEM (JSM-6701F) was used to test the sandstone samples after 0, 3, 5, 10, 15, and 20 cycles.

Figure 3 shows the SEM images after different WD cycles. For the sample without WD cycles (Fig. 3a), the surface of the sandstone is flat. The cementation between mineral particles is solid, and the microstructure is dense. There are few pores without obvious particle boundary. However, irreversible damage occurs after the WD cycles. With the increase of cycles, curling phenomenon occurs with the plane changing from flat to uneven. The size and number of pores gradually increase (Fig. 3a–f). With the increasing cycles, the degree of cementation between particles decreases, the microstructure becomes more loose and broken, and there are more flaky and scaly blocks. After 20 cycles (Fig. 3f), the microstructure of sandstone has been significantly deteriorated. Thus, the strength of sandstone samples will be affected.

According to the mineral composition content (Fig. 1), sandstone contains quartz (SiO_2), calcite ($CaCO_3$), and albite ($NaAlSi_3O_8$). During the wetting process, complex dissolution reaction occurs since minerals of the sandstone are exposed to water. The detailed reaction equations are shown in Eqs. (1)–(3) (Liu et al. 2016b, 2018b).

$$CaCO_3 = Ca^{2+} + CO_3^{2-} \tag{1}$$

Table 2 Screening criteria for samples

Detection item	Height	End face parallelism	Vertical axis of end face	Wave velocity
Error limit	<0.2 mm	<0.05 mm	<0.25°	<5%

Fig. 2 Prepared samples

$$NaAlSi_3O_8 + 5.5H_2O = 0.5Al_2Si_2O_5(OH)_4 + Na^+ + OH^- + 2H_4SiO_4 \tag{2}$$

$$SiO_2 + 2H_2O = H_4SiO_4 \tag{3}$$
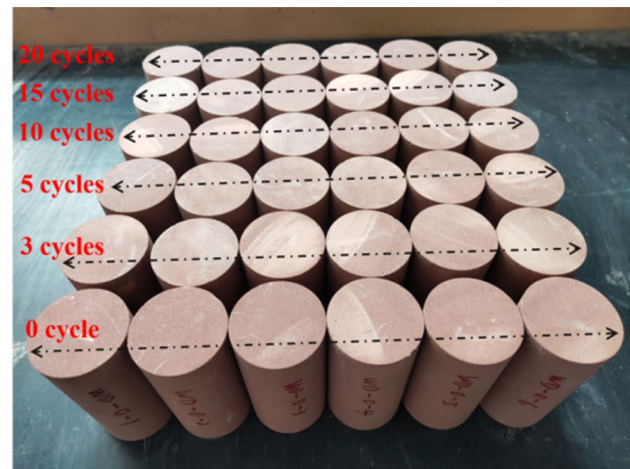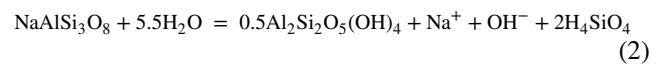
Figure 4 shows the mineral compositions of sandstone samples after 20 cycles. From 0 to 20 cycles, the proportion of calcite in mass reduces from 19.7% to 9.3% due to the dissolution of calcite in Eq. (1). The proportion of albite in mass reduces from 23.1% to 19.8% due to the dissolution of albite in Eq. (2). Among the three minerals, calcite has the strongest solubility, and the solubility of quartz is very small (Liu et al. 2018b; Feng et al. 2010). Therefore, the proportion of quartz in mass becomes larger (from 57.2% to 70.9%) after 20 cycles.

Meanwhile, the reaction can produce new pores which will connect with original pores within the natural sandstone. The connectivity between pores provides more reaction surfaces for water–rock interaction and further promotes the deterioration of the microstructure. During the drying process, loose particles produced by water–rock interaction leak out along the pores in the process of water infiltration and transportation, and causes secondary pores. This also provides more contact space for the water–rock interaction, and the microstructure deteriorates to a greater degree during the next wetting process. Therefore, the microstructure damage gradually increases after repeated WD cycles. The accumulation of microstructure variation can cause the mesoscopic response of sandstone.

3.2 Analysis of Meso–micro Pore Characteristics

To reveal the meso–micro pore response within sandstone, the low-field NMR technique was selected to measure the pore size and distribution after different WD cycles.
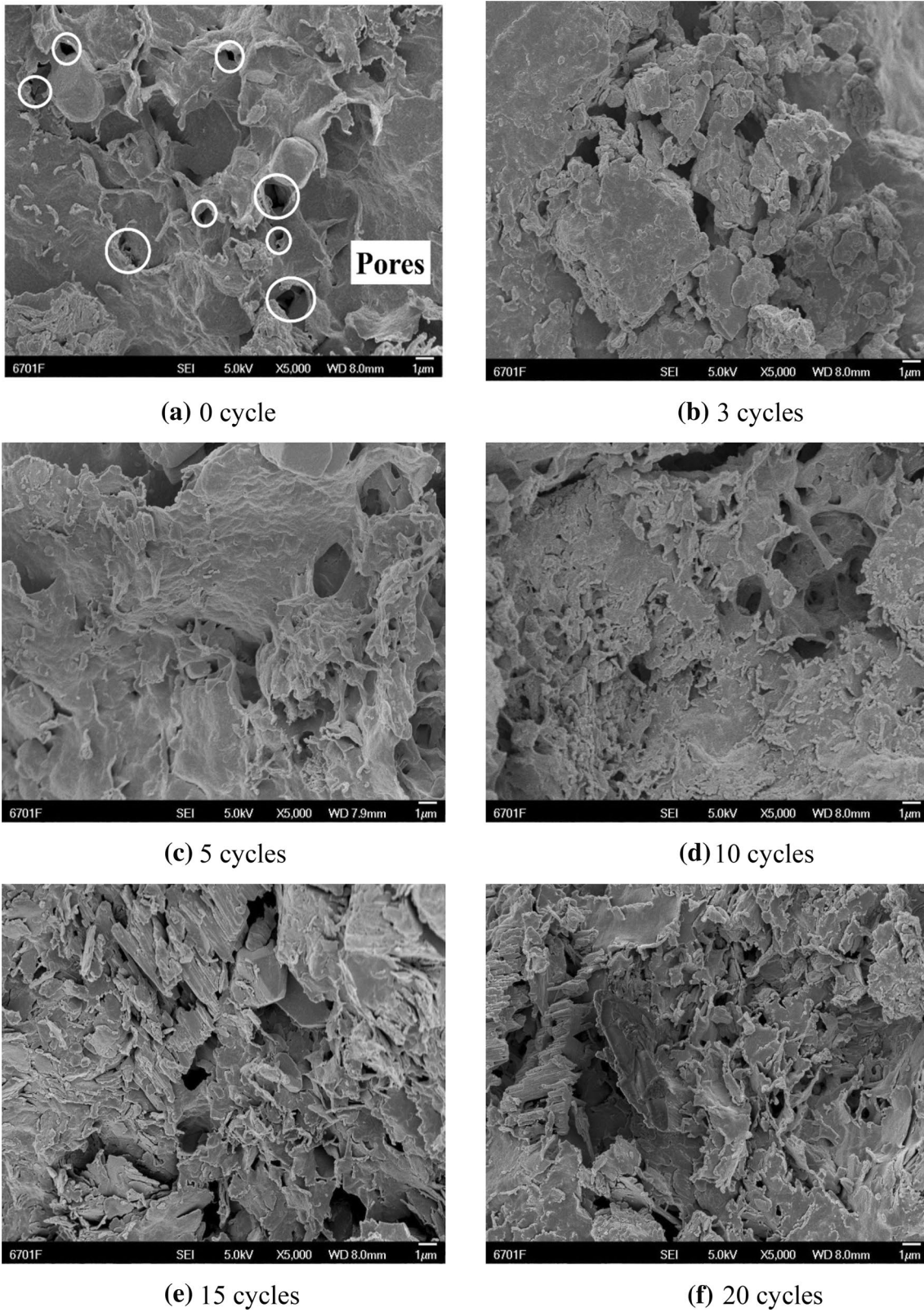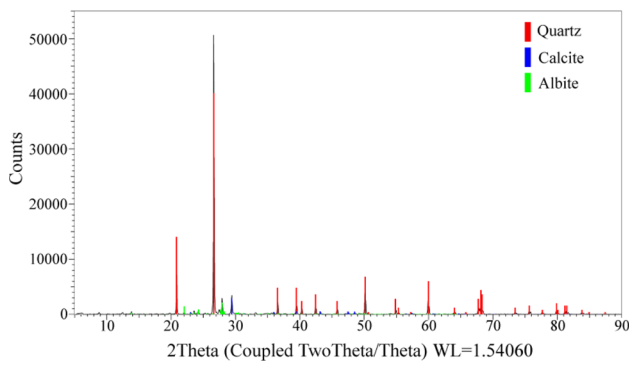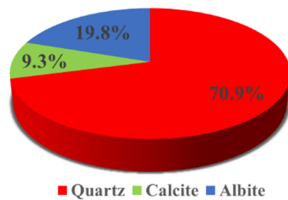
(a) 0 cycle

(b) 3 cycles

(c) 5 cycles

(d) 10 cycles

(e) 15 cycles

(f) 20 cycles

Fig. 3 SEM images for the surfaces of sandstone samples after different WD cycles (×5000)

(a) Diagram of the X-ray analysis

(b) Mineral composition proportion

Fig. 4 Energy spectrum analysis results of sandstone after 20 cycles

Fig. 5 Variation of porosity after different WD cycles

Meanwhile, CT scanning technology was also used to quantitatively and qualitatively analyze the variation of mesoscopic structure.

3.2.1 NMR Tests

The pores could significantly influence the physical and mechanical properties of sandstone (Ju et al. 2013). To analyze the influence of WD cycles on the pore characteristics, e.g., size, porosity, content and pore throat, the MiniMR60 system was used.

(1) Principle of NMR

NMR measures the pore characteristics by testing the relaxation time of water within the pore. The total transverse relaxation rate $\left(\frac{1}{T_2}\right)$ can be expressed as follows (Rylander et al. 2013; Toumelin et al. 2007):

$$\frac{1}{T_2} = \frac{1}{T_{2S}} + \frac{1}{T_{2D}} + \frac{1}{T_{2B}}, \tag{4}$$

where T_2 is the total lateral relaxation time, T_{2S} is the lateral relaxation time of fluid caused by surface relaxation, T_{2D} is the lateral relaxation time of fluid caused by diffusion relaxation under gradient magnetic field, and T_{2B} is the lateral relaxation time of the free state fluid. In the tests, the total lateral relaxation time T_2 mainly depends on the surface
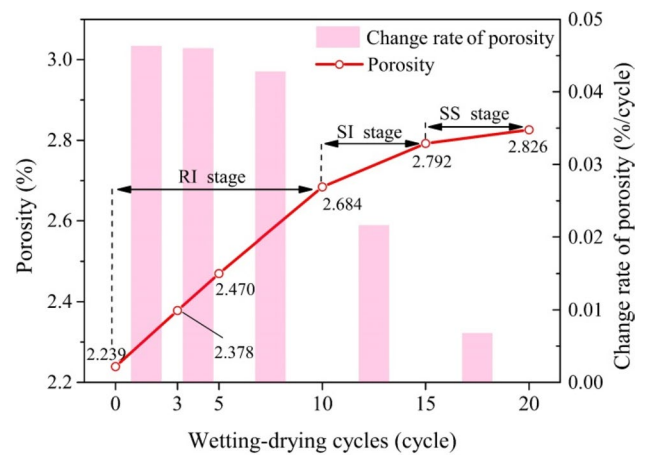
relaxation. Thus, the T_{2D} and T_{2B} can be ignored (Shen et al. 2020). T_{2S} can be calculated by Eq. (5):

$$T_{2S} = \frac{1}{\rho_2 \left(\frac{S}{V}\right)_{\text{pore}}}, \tag{5}$$

where ρ_2 is the T_2 surface relaxivity, S is surface area of the pore, and V is the pore volume.

Therefore, Eq. (4) can be simplified to Eq. (6) (Müller-Huber et al. 2016; Kleinberg et al. 1994):

$$\frac{1}{T_2} = \rho_2 \left(\frac{S}{V}\right)_{\text{pore}}. \tag{6}$$

For the spherical pore and columnar pore, Eq. (6) can be further transformed as:

$$r = T_2 \rho_2 F_s, \tag{7}$$

where r is the pore radius, and F_s is the geometric factor.

For specific sandstone, $\rho_2 F_s$ is a constant value, and its range is 0.01–0.15 μm/ms (Li et al. 2018). Therefore, the pore radius r increases with relaxation time T_2. In this study, $\rho_2 F_s$ is taken as 0.02 μm/ms.

(2) NMR results

Figure 5 quantitatively shows the variation of porosity after different WD cycles. The initial porosity is 2.239%. With the increasing cycles, the porosity nonlinearly increases due to the repeated water–rock action. The variation process is consistent with the qualitative change of microstructure (Fig. 3). However, the change rate of porosity decreases with WD cycles. It indicates that the damage effect of WD cycles constantly decreases and the pore structure tends to be stable. In addition, there are three obvious stages for the variation of porosity. During the first stage (RI stage: 0–10 cycles), the porosity rapidly increases from the initial value 2.239% to 2.684% with the change rates are more than

0.04% for every cycle. In the second stage (SI stage: 10–15 cycles), the change rate slows down to 0.0216% for every cycle. After 15 cycles (SS stage: the third stage), the porosity tends to be stable with the change rate of 0.0068% for every cycle.

The content of soluble minerals contributes to the porosity change under WD cycles. Dissolution reaction occurs when water infiltrates into samples, and new pores caused by water–rock action will accelerate the mineral dissolution. However, it can be seen that after 20 cycles, although there are still a large number of soluble minerals in the sandstone (Fig. 4), the porosity and its change tend to be stable (Fig. 5). This is mainly because the dense sandstone with small initial porosity (2.239%) limited the further water's infiltrating quality and water–rock action. Thus, the change rate of porosity slows down after certain WD cycles, and the certain value depends on both the dense degree and content of soluble mineral. In the tests, the certain cycle is nearly 10.

Figure 6 shows the curves of the pore content and pore proportion after different cycles. The WD cycles changes the pore structure. From 0 to 20 cycles, the pore size range varies from 0.00053–18.6521 μm to 0.00046–49.5415 μm. This is mainly due to the formation of new pores and extension of original pores. According to the existing literature (Shen et al. 2020; Zhang et al. 2019b; Yan et al. 2016), the pore size can be divided into three types, including the small pores (< 0.1 μm), middle pores (0.1–1 μm), and large pores (> 0.1 μm). It can be obtained from Fig. 6 that the pores in sandstone are mainly constituted by small pores, followed by middle pores, and the large pores are the least. In addition, the size for the most probable pore (MPP) of sandstone under different cycles is always approximately 0.02 μm, and

the proportion of the MPP decreases with the increasing cycles (Fig. 6b). Its proportion decreases from 5.47% for 0 cycle to 4.70% for 20 cycles.

To clearly show the variations of pores, we list the pore content and corresponding proportion of three kinds of pores after different WD cycles (Fig. 7). Although the WD cycles affect the pore structure during 20 cycles, the content and proportion of the small pores are still the highest, followed by the middle pores, and the large pores are the least. With the increase of the cycles, the content of small pores gradually increases, but its proportion decreases. For middle pores, its content and proportion increase in the first 5 cycles. After 10 cycles, they decrease and then gradually increase. On the whole, the porosity and proportion of the middle pores shows the law of growth. Meanwhile, the content and proportion of large pores continuously increase with the increase of the cycles. Hence, the change of pore structure under the WD cycles actually includes the formation of new small pores, and the connection and extension of original pores.

Pore throat (PT) is also an important index of pore structure. The PT represents the interconnected and narrow passage between the pores. Figure 8 shows the PT distribution of sample under different numbers of WD cycles. The proportion of the PTs less than 0.1 μm is always the largest, and it decreases with the increase of the cycles. After 20 cycles, it decreases from the initial value of 91.53% to 84.52%. Almost all the proportion of the PTs groups (> 4 μm) increase with the cycles. The phenomena also indicate that the original small PTs can connect and extend into larger PTs. However, there is no obvious law for the proportion of PTs with the size of 0.1–4 μm.
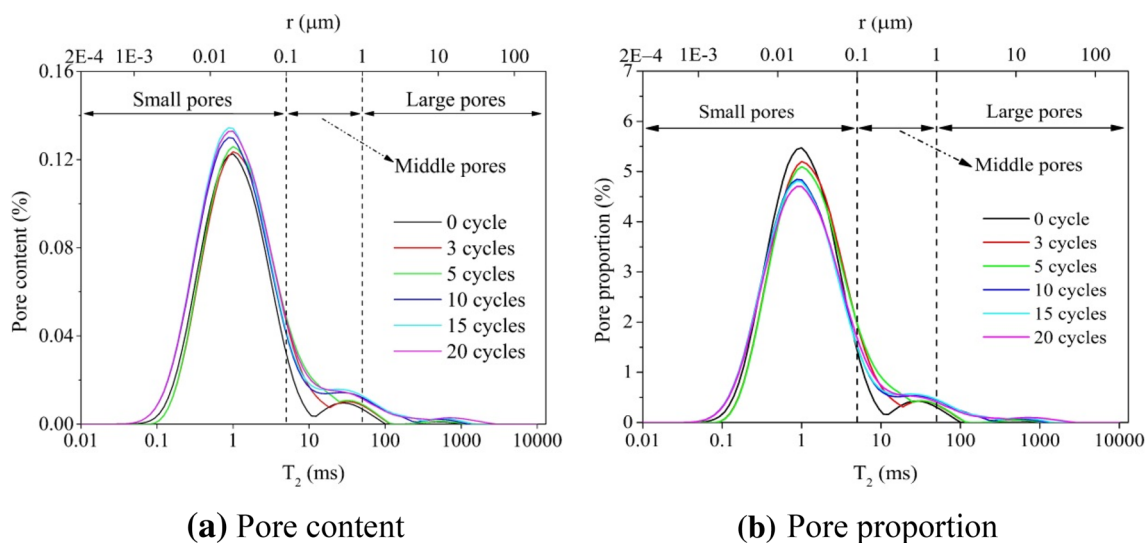

(a) Pore content

(b) Pore proportion

Fig. 6 Pore content and pore proportion curves after different numbers of WD cycles
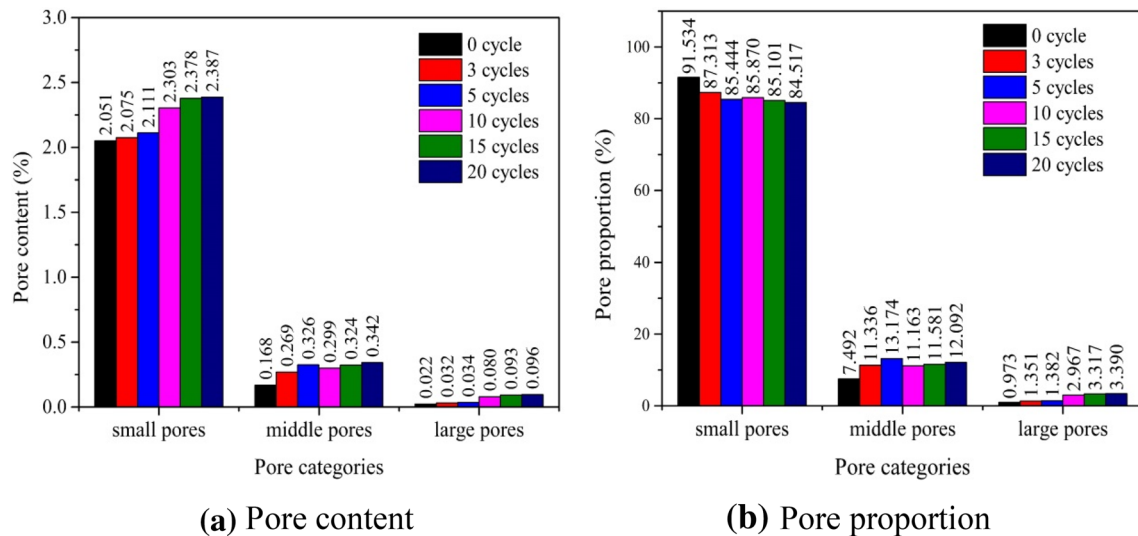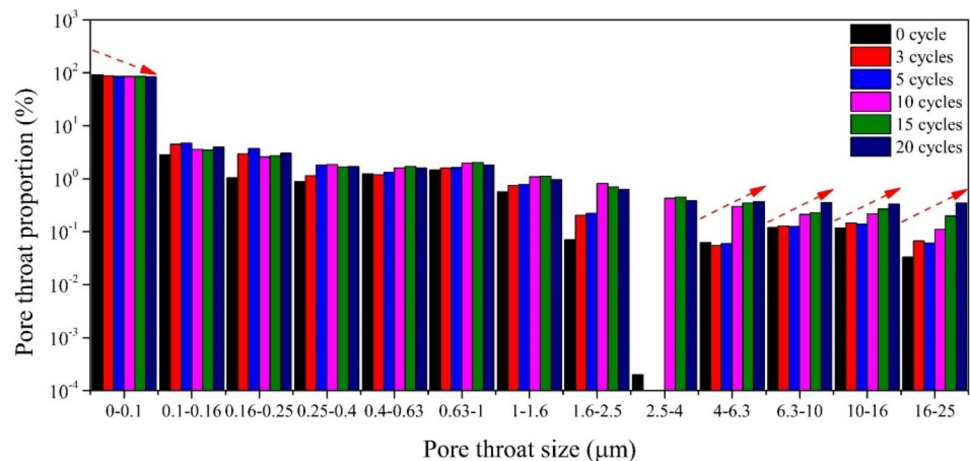
(a) Pore content

(b) Pore proportion

Fig. 7 Pore content and pore proportion after different numbers of WD cycles

Fig. 8 Proportion change of pore throat after different numbers of WD cycles


3.2.2 CT Test

Philips Brilliance 16 multi energy spiral CT machine with a spatial resolution of 0.208 mm and a density resolution of 0.3% was used. The scanning interval between adjacent cross sections is 3 mm, and each sample is scanned with 33 sections every time. CT scanning images can reflect the density distribution of sandstone sample. The scanning images of one same cross section after different cycles are selected (Fig. 9). In CT scanning images, the black color refers to the low-density area, and the white color represents the high-density area. With the increase of WD cycles, the black areas become significant in local region, and the decrease of sample density is mainly due to the increase of the porosity. The continuous deterioration of density forms several distinct band-shaped low-density areas within the sample, especially after 5 cycles (Fig. 9c–f). As the number of cycles increases,

the band-shaped low-density area continues to expand and extend, and two obvious band-shaped low-density regions appear on the cross section after 20 cycles (Fig. 9f).

The value of each pixel point in the scanning image is the CT number which is proportional to the corresponding density of sandstone (Liu et al. 2016a). The mean of CT number (MCT) is positively related to the density. The standard deviation of CT number (SDCT) reflects the discreteness of the density. Because the scanning results of a single section can only reflect the information of specific section, it cannot reflect the information of the overall sample. To describe the density variation of the whole sandstone sample, the MCT and SDCT for all scanning sections under same cycles are shown in Fig. 10.

The MCT and its change rate within the process of adjacent designed cycles are shown in Fig. 10a. It can be seen that the MCT decreases with the increase of cycles, which

Fig. 9 CT scanning images

(a) 0 cycle   **(b)** 3 cycles   **(c)** 5 cycles

(d) 10 cycles   **(e)** 15 cycles   **(f)** 20 cycles
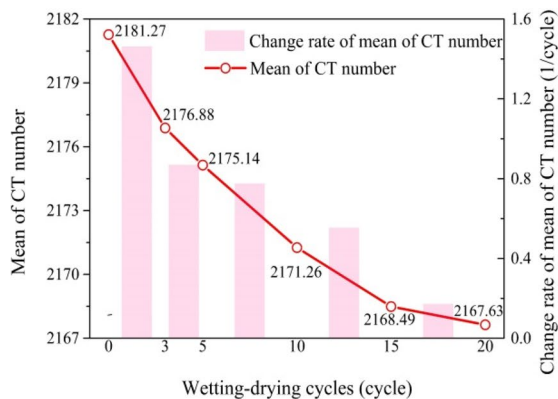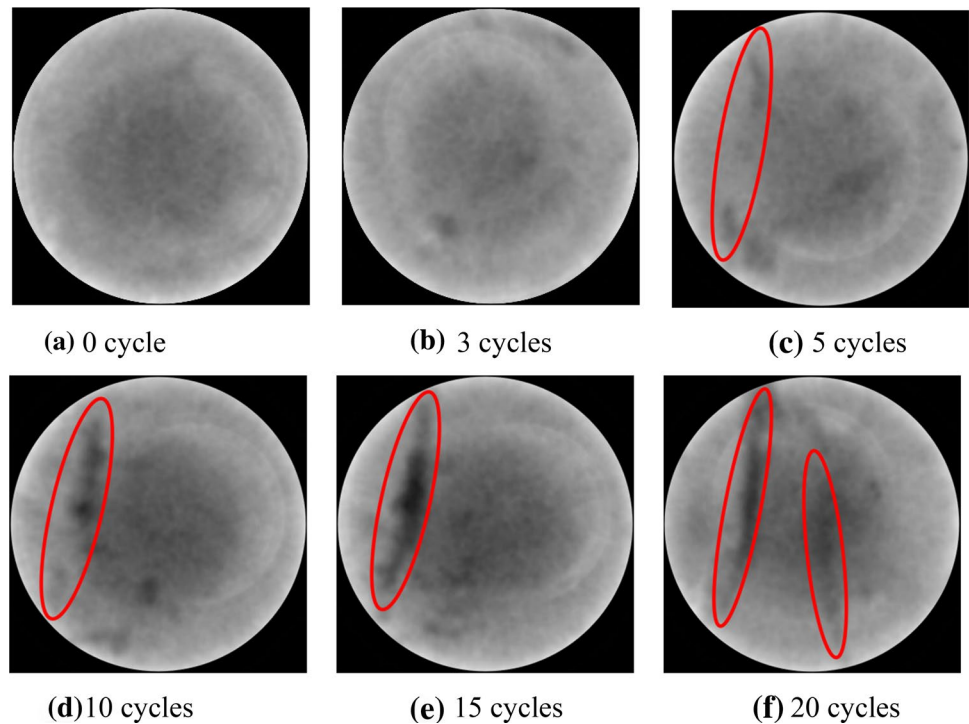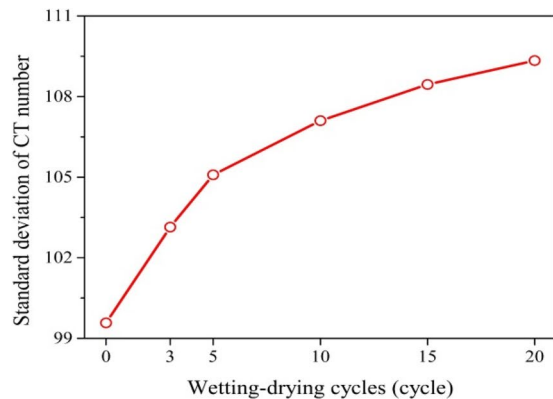
(a) Mean of CT number   **(b)** Standard deviation of the CT number

Fig. 10 CT numbers of samples under different numbers of WD cycles

is mainly due to the deterioration of pore structure caused by the WD cycles. Therefore, the density decreases with the increase of the cycles. Within 0–3, 3–5, 5–10, 10–15, and 15–20 cycles, the change rates of MCT are 1.46, 0.87, 0.78, 0.55, and 0.17, respectively. The results show that when the number of cycles is less, the damage effect of WD cycles on sandstone is significant. Although the influence of the WD cycles on the sandstone decreases as the number of cycles increases, the continuously increasing SDCT (Fig. 10b) illustrates that the spatial differentiation of density becomes obvious due to the formation of low-density areas.

3.3 Analysis of Macroscopic Physical and Mechanical Properties

The structure of the sandstone gradually deteriorates from the micro-scale to the meso-scale under the action of WD cycles, and then some performance degradation phenomena will occur on the macro-scale. Therefore, in order to understand the influence of WD cycles on the macroscopic physical and mechanical properties of sandstone, we carried out ultrasonic tests and uniaxial compression tests, respectively.

3.3.1 Ultrasonic Tests

To explore the influence of WD cycles on the compactness of sandstone, ultrasonic test was performed after designed cycles. According to Eqs. (8) and (9) (DL/T 5368-2007), the dynamic elastic modulus $\left(E_d\right)$ can be obtained by the P-wave velocity and the S-wave velocity:

$$\mu = \frac{\left(\frac{V_p}{V_s}\right)^2 - 2}{2\left[\left(\frac{V_p}{V_s}\right)^2 - 1\right]}, \tag{8}$$

$$E_d = 2\rho V_s^2(1 + \mu) \times 10^{-3}, \tag{9}$$

where ρ is the density, V_p is the P-wave velocity, and V_s is the S-wave velocity.

The change of P-wave velocity, S-wave velocity, dynamic elastic modulus and corresponding change rates within the process of adjacent designed cycles are shown in Fig. 11a–c, respectively. It can be seen that P-wave velocity, S-wave velocity, and dynamic elastic modulus all decrease with the increase of cycles. The main reason is that WD cycles increase the porosity, which in turn reduce the compactness of sandstone samples. Meanwhile, the change rates of the three parameters also decrease with cycles. This is mainly because when the number of cycles is less, the damage caused by the WD cycles is larger, and the compactness of the samples decreases more. As the cycles increase, the new damage decreases, and the compactness of the sandstone tends to be stable, so the reduction rates of the three parameters gradually decrease. In addition, the change rate of the P-wave velocity is more significant than that of the S-wave velocity, especially in the first 5 cycles. Consequently, the structure deterioration caused by the WD cycles has the small influence on the S-wave velocity.

3.3.2 Uniaxial Compression Tests

The uniaxial compression tests were conducted to explore the influence of WD cycles on the macroscopic mechanical properties of sandstone. According to the Test Methods of
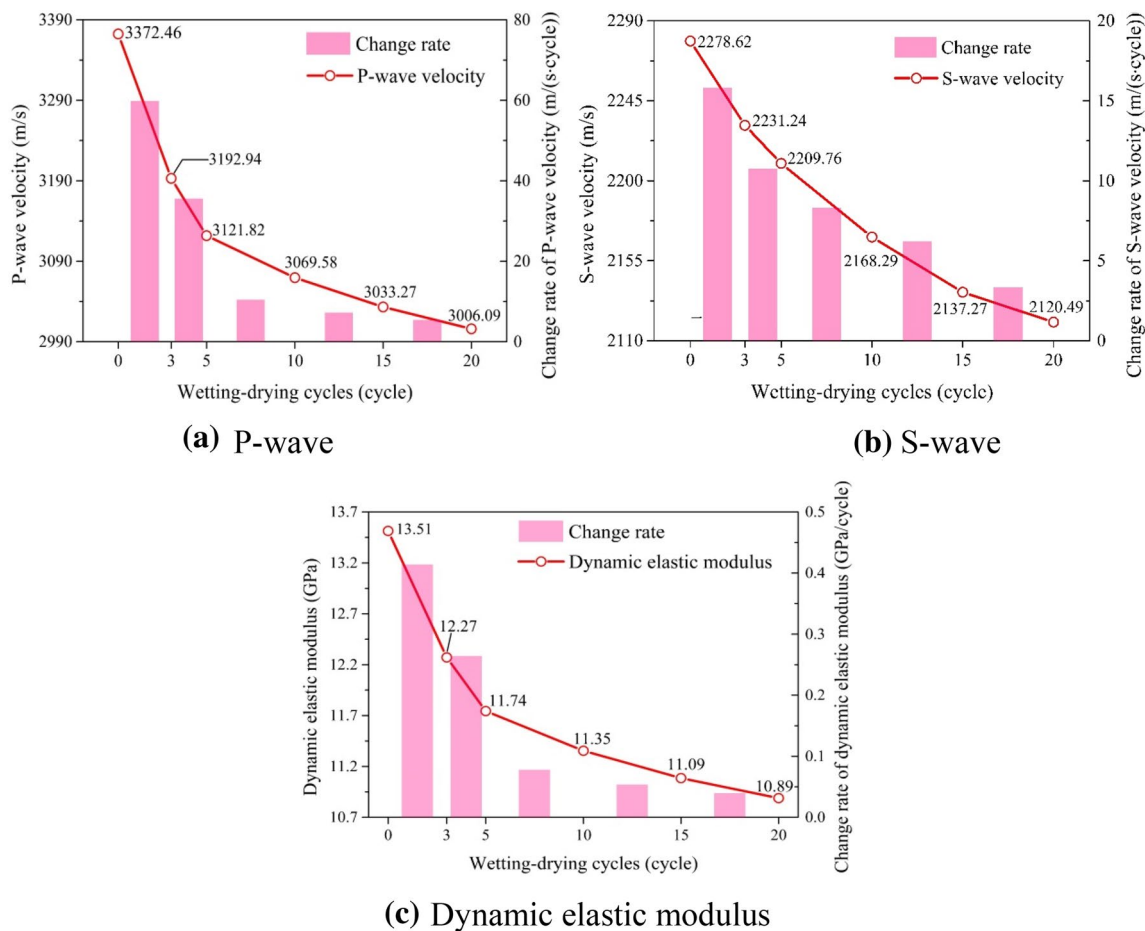

(a) P-wave

(b) S-wave

(c) Dynamic elastic modulus

Fig. 11 Change of P-wave velocity, S-wave velocity, and dynamic elastic modulus under different numbers of WD cycles

Rock for Highway Engineering (JTG E41-2005) and Code for rock tests in water and hydropower projects (SL/T 264-2020), the loading rate of uniaxial compression tests is set at 0.5 MPa/s. The typical failure patterns of the sandstone samples after different cycles are shown in Fig. 12. The obvious tensile failure can be seen after the uniaxial compression tests, and there are many macroscopic fracture surfaces.

Figure 13 shows the stress–strain curves of samples under different cycles. All curves have five stages (Cai 2002; Martin and Chandler 1994) (only the curve of 0 cycle is marked), including (1) pore compaction stage (OA stage) with a up concave shape in the curves: the pores of the sandstone sample gradually close under compression during this stage; (2) elastic deformation stage (AB stage): during this stage, the stress linearly increases with strain; (3) stable crack growth stage (BC stage): The cracks begin to form at this stage; (4) unstable crack growth stage (CD stage) with a down concave shape in the stress–strain curves: the formation speed of cracks inside the sandstone increases, and the distribution of cracks becomes dense. The sandstone reaches its peak stress at point *D*; (5) post-peak stage (DE stage): after the sandstone reaches the peak stress, the cracks rapidly form, intersect, and develop to macroscopic fracture surfaces (Fig. 12). The stress of sandstone rapidly decreases with the increase of strain. The slope of this stage in the stress–strain curve is negative.

Although the shape of all stress–strain curves is similar, the detailed characteristics vary with WD cycles. The strain at the end of compaction stage increases with WD cycles. The pore compaction stage is longer for sandstone with more cycles due to the increase of porosity caused by the WD cycles. Meanwhile, the peak strain also increases with the increase of cycles. When the cycle varies from 0 to 20, the value of the peak strain increases from 0.00914 to 0.01075. The reason is that the aggravation of damage caused by WD cycles results in the lengthening of compaction stage.
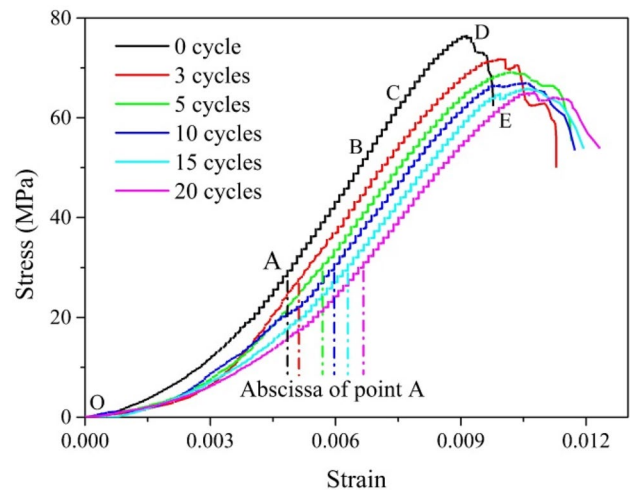

Fig. 13 Stress–strain curves of different cycles

In addition, the UCS of the sandstone gradually decreases under the increasing WD cycles (Fig. 14). The deterioration of the UCS is obvious in the first 5 cycles. It reduces from 76.35 MPa without WD cycles to 69.10 MPa after 5 cycles. Meanwhile, the decrease rate within the process of adjacent designed cycles of the UCS gradually falls down with the increasing cycles. The deterioration process of elastic modulus (E) is similar to that of the UCS. From the change law of UCS and E, it can be concluded that the WD cycles deteriorate the mechanical properties of sandstone, and the effect of degradation gradually decreases with the increasing cycles. To obtain the detailed relationship between the UCS and E with the WD cycles, nonlinear regression is conducted. The regression equations (10) and (11) show that both the UCS and the E exponentially decrease with WD cycles, and the correlation coefficients (R^2) are 0.996 and 0.991, respectively,
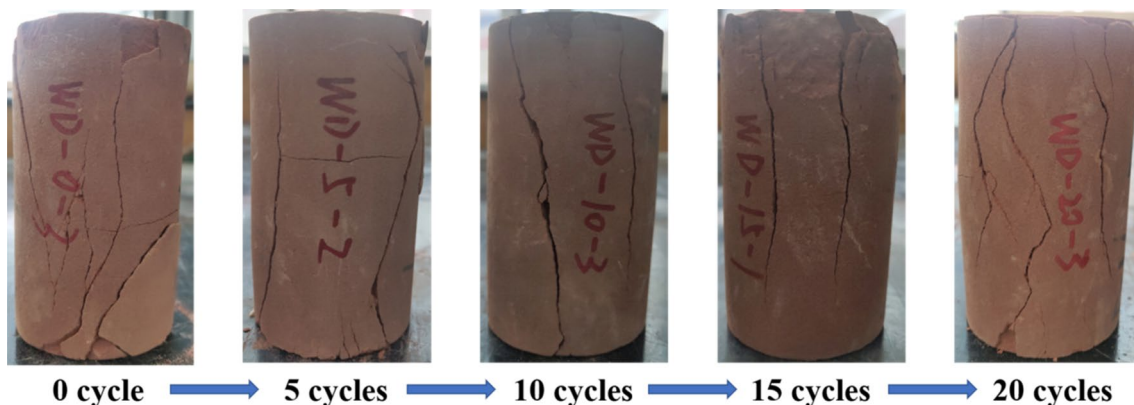

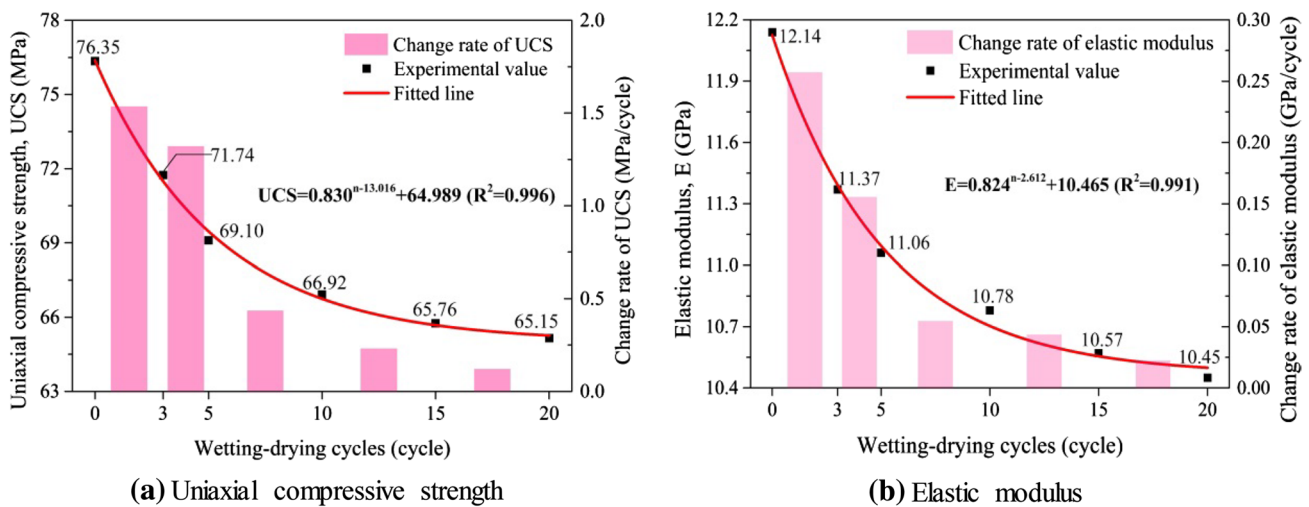**Fig. 12** Failure patterns of sandstone under uniaxial compression

Fig. 14 Change of uniaxial compressive strength and elastic modulus under different numbers of WD cycles

$$\text{UCS} = 0.830^{n-13.016} + 64.989, \tag{10}$$

$$E = 0.824^{n-2.612} + 10.465. \tag{11}$$

4 Conclusions

In this study, we systematically analyze the deterioration mechanism of wetting–drying (WD) cycles on the sandstone by combining the microstructure change, the variation of meso–micro pore characteristics, and the macroscopic physical and mechanical properties. Based on the experimental investigations, several conclusions can be drawn as follows:

1. The WD cycles deteriorate microstructure of sandstone due to the dissolution reaction of dissolved minerals. The content of dissolved minerals and the permeability of sandstone are the two key factors that determine degradation influence of WD cycles.

2. WD cycles change the size and content of pores in sandstone. The porosity of the sandstone sample increases with the increasing WD cycles. The WD cycles makes the pore size range wider due to the formation of new small pores and the connection and extension of original pores. For the sandstone in the tests, initial pore size range varies from 0.00053–18.6521 μm to 0.00046–49.5415 μm after 20 WD cycles.

3. The change of pore structure affects the density distribution within the sandstone. With the increasing WD cycles, both the density and its change rate reduce, and the density dispersion of sandstone increases.

4. The growth of porosity caused by WD cycles weakens the physical and mechanical properties of the sandstone, including the P-wave velocity, S-wave velocity, dynamic elastic modulus, uniaxial compressive strength and elastic modulus. Finally, exponential formulas are established to describe the relationship of the uniaxial compressive strength and the elastic modulus with the number of WD cycles.

Compliance with Ethical Standards

Conflict of interest The authors declare that they have no conflict of interest.

References

Cai MF (2002) Rock mechanics and engineering. Science Press, Beijing

Cai X, Zhou Z, Tan L, Zang H, Song Z (2020) Fracture behavior and damage mechanisms of sandstone subjected to wetting-drying cycles. Eng Fract Mech 234:107109. https://doi.org/10.1016/j.engfracmech.2020.107109

Chen YF, Ai ZY (2020) Viscoelastic analysis of transversely isotropic multilayered porous rock foundation by fractional

Poynting-Thomson model. Eng Geol 264:105327. https://doi.org/10.1016/j.enggeo.2019.105327

de Argandoña VGR, Rey AR, Celorio C, del Río LMS, Calleja L, Llavona J (1999) Characterization by computed X-ray tomography of the evolution of the pore structure of a dolomite rock during freeze-thaw cyclic tests. Phys Chem Earth Part A Solid Earth Geodyn 24:633–637. https://doi.org/10.1016/S1464-1895(99)00092-7

Dehestani A, Hosseini M, Beydokhti AT (2020) Effect of wetting–drying cycles on mode I and mode II fracture toughness of sandstone in natural (pH = 7) and acidic (pH = 3) environments. Theor Appl Fract Mech 107:102512. https://doi.org/10.1016/j.tafmec.2020.102512

Feng XT, Ding XW, Cui Q (2010) Coupled chemical-effect on rock fracturing process. Science Press, Beijing

Hale PA, Shakoor A (2003) A laboratory investigation of the effects of cyclic heating and cooling, wetting and drying, and freezing and thawing on the compressive strength of selected sandstones. Environ Eng Geosci 9:117–130. https://doi.org/10.2113/9.2.117

Hua W, Dong SM, Li YF, Xu JG, Wang QY (2015) The influence of cyclic wetting and drying on the fracture toughness of sandstone. Int J Rock Mech Min Sci 78:331–335. https://doi.org/10.1016/j.ijrmms.2015.06.010

Hua W, Dong SM, Peng F, Li KY, Wang QY (2017) Experimental investigation on the effect of wetting-drying cycles on mixed mode fracture toughness of sandstone. Int J Rock Mech Min Sci 93:242–249. https://doi.org/10.1016/j.ijrmms.2017.01.017

Ju Y, Yang YM, Peng RD, Mao LT (2013) Effects of pore structures on static mechanical properties of sandstone. J Geotech Geoenviron Eng 139:1745–1755. https://doi.org/10.1061/(ASCE)GT.1943-5606.0000893

Khanlari G, Abdilor Y (2015) Influence of wet–dry, freeze–thaw, and heat–cool cycles on the physical and mechanical properties of Upper Red sandstones in central Iran. Bull Eng Geol Environ 74:1287–1300. https://doi.org/10.1007/s10064-014-0691-8

Kleinberg RL, Kenyon WE, Mitra PP (1994) Mechanism of NMR relaxation of fluids in rock. J Magn Reson Ser A 108:206–214. https://doi.org/10.1006/jmra.1994.1112

Lai YM, Zhang MY, Li SY (2009) Theory and application of cold regions engineering. Science Press, Beijing

Li JL, Zhou KP, Liu WJ, Deng HW (2016) NMR research on deterioration characteristics of microscopic structure of sandstones in freeze–thaw cycles. Trans Nonferrous Met Soc China 26:2997–3003. https://doi.org/10.1016/S1003-6326(16)64430-8

Li JL, Kaunda RB, Zhou KP (2018) Experimental investigations on the effects of ambient freeze-thaw cycling on dynamic properties and rock pore structure deterioration of sandstone. Cold Reg Sci Technol 154:133–141. https://doi.org/10.1016/j.coldregions.2018.06.015

Liu XR, Zijuan W, Yan F, Wen Y, Luli M (2016a) Macro/microtesting and damage and degradation of sandstones under dry-wet cycles. Adv Mater Sci Eng 2016:1–16

Liu XR, Yuan W, Fu Y, Wang ZJ, Miao LL, Xie WB (2016b) Tests on shear strength deterioration of sandstone under the action of chemical solution and drying-wetting cycles and analysis of chemical thermodynamics. Chin J Rock Mech Eng 35:2534–2541

Liu XR, Jin MH, Li DL, Zhang L (2018a) Strength deterioration of a Shaly sandstone under dry–wet cycles: a case study from the Three Gorges Reservoir in China. Bull Eng Geol Environ 77:1607–1621. https://doi.org/10.1007/s10064-017-1107-3

Liu XR, Yuan W, Fu Y, Wang ZJ, Miao LL, Xie WB (2018b) Porosity evolution of sandstone dissolution under wetting and drying cycles. Chin J Geotech Eng 40:527–532. https://doi.org/10.11779/CJGE201803017

Liu B, Ma YJ, Liu N, Han Y, Li DY, Deng HL (2019) Investigation of pore structure changes in Mesozoic water-rich sandstone induced by freeze-thaw process under different confining pressures using

digital rock technology. Cold Reg Sci Technol 161:137–149. https://doi.org/10.1016/j.coldregions.2019.03.006

Lu Y, Li X, Chan A (2019) Damage constitutive model of single flaw sandstone under freeze-thaw and load. Cold Reg Sci Technol 159:20–28. https://doi.org/10.1016/j.coldregions.2018.11.017

Lv Z, Xia C, Wang Y, Luo J (2019) Analytical elasto-plastic solution of frost heaving force in cold region tunnels considering transversely isotropic frost heave of surrounding rock. Cold Reg Sci Technol 163:87–97. https://doi.org/10.1016/j.coldregions.2019.04.008

Martin CD, Chandler NA (1994) The progressive fracture of Lac du Bonnet granite. Int J Rock Mech Min Sci 31:643–659. https://doi.org/10.1016/0148-9062(94)90005-1

Müller-Huber E, Schön J, Börner F (2016) Pore space characterization in carbonate rocks—approach to combine nuclear magnetic resonance and elastic wave velocity measurements. J Appl Geophys 127:68–81. https://doi.org/10.1016/j.jappgeo.2016.02.011

Özbek A (2014) Investigation of the effects of wetting-drying and freezing-thawing cycles on some physical and mechanical properties of selected ignimbrites. Bull Eng Geol Environ 73:595–609. https://doi.org/10.1007/s10064-013-0519-y

Pardini G, Guidi GV, Pini R, Regüés D, Gallart F (1996) Structure and porosity of smectitic mudrocks as affected by experimental wetting-drying cycles and freezing-thawing cycles. CATENA 27:149–165. https://doi.org/10.1016/0341-8162(96)00024-0

Pei WS, Zhang MY, Li SY, Lai YM, Jin L (2017) Thermo-mechanical stability analysis of cooling embankment with crushed-rock interlayer on a sloping ground in permafrost regions. Appl Therm Eng 125:1200–1208. https://doi.org/10.1016/j.applthermaleng.2017.07.105

Qin Z, Chen X, Fu H (2018) Damage features of altered rock subjected to drying-wetting cycles. Adv Civ Eng 2018:1–10. https://doi.org/10.1155/2018/5170832

Rylander E, Singer PM, Jiang T, Lewis R, McLin R, Sinclair S (2013) NMR T2 distributions in the Eagle Ford shale: reflections on pore size. Soc Pet Eng SPE USA Unconv Resour Conf 2013:426–440. https://doi.org/10.2118/164554-ms

Shen YJ, Wang YZ, Wei X, Jia HL, Yan RX (2020) Investigation on meso-debonding process of the–concrete interface induced by freeze–thaw cycles using NMR technology. Constr Build Mater 2020:252. https://doi.org/10.1016/j.conbuildmat.2020.118962

Shi S, Zhao R, Li S, Xie X, Li L, Zhou Z, Liu H (2019) Intelligent prediction of surrounding rock deformation of shallow buried highway tunnel and its engineering application. Tunn Undergr Sp Technol 90:1–11. https://doi.org/10.1016/j.tust.2019.04.013

Song DQ, Che AL, Chen Z, Ge XR (2018) Seismic stability of a rock slope with discontinuities under rapid water drawdown and earthquakes in large-scale shaking table tests. Eng Geol 245:153–168. https://doi.org/10.1016/j.enggeo.2018.08.011

Song YJ, Zhang LT, Ren JX, Chen JX, Che YX, Yang HM, Bi R (2019) Study on damage characteristics of weak cementation sandstone under drying-wetting cycles based on nuclear magnetic resonance technique, Yanshilixue Yu Gongcheng Xuebao/Chinese. J Rock Mech Eng 38:825–831. https://doi.org/10.13722/j.cnki.jrme.2018.1412

Sun Y, Zhai C, Xu JZ, Cong YZ, Qin L, Zhao C (2020) Characterisation and evolution of the full size range of pores and fractures in rocks under freeze-thaw conditions using nuclear magnetic resonance and three-dimensional X-ray microscopy. Eng Geol 271:105616. https://doi.org/10.1016/j.enggeo.2020.105616

Tai BW, Wu QB, Zhang ZQ, Xu XM (2020) Cooling performance and deformation behavior of crushed-rock embankments on the Qinghai-Tibet Railway in permafrost regions. Eng Geol 2020:265. https://doi.org/10.1016/j.enggeo.2019.105453

Takano D, Lenoir N, Otani J, Hall SA (2015) Localised deformation in a wide-grained sand under triaxial compression revealed by

X-ray tomography and digital image correlation. Soils Found 55:906–915. https://doi.org/10.1016/j.sandf.2015.06.020

Tang J, Liu YB (2012) Bearing capacity calculation of rock foundation based on nonlinear failure criterion. IERI Procedia 1:110–116. https://doi.org/10.1016/j.ieri.2012.06.018

Torres-Suarez MC, Alarcon-Guzman A, Berdugo-De RM (2014) Effects of loading-unloading and wetting-drying cycles on geomechanical behaviors of mudrocks in the Colombian Andes. J Rock Mech Geotech Eng 6:257–268. https://doi.org/10.1016/j.jrmge.2014.04.004

Toumelin E, Torres-Verdín C, Sun B, Dunn KJ (2007) Random-walk technique for simulating NMR measurements and 2D NMR maps of porous media with relaxing and permeable boundaries. J Magn Reson 188:83–96. https://doi.org/10.1016/j.jmr.2007.05.024

Wang Y, Li X, Zhang B, Wu YF (2014) Meso-damage cracking characteristics analysis for rock and soil aggregate with CT test. Sci China Technol Sci 57:1361–1371. https://doi.org/10.1007/s11431-014-5578-1

Xie KN, Jiang DY, Sun ZG, Song ZQ, Wang JY, Yang T, Jiang X (2019) Influence of drying-wetting cycles on microstructure degradation of argillaceous sandstone using low field nuclear magnetic resonance. Yantu Lixue/Rock Soil Mech. 40:653–659, 667. https://doi.org/10.16285/j.rsm.2017.1436

Xu JS, Yang XL (2018) Seismic stability analysis and charts of a 3D rock slope in Hoek-Brown media. Int J Rock Mech Min Sci 112:64–76. https://doi.org/10.1016/j.ijrmms.2018.10.005

Yan JP, Wen DN, Li ZZ, Geng B, Cai JG, Liang Q, Yan Y (2016) The quantitative evaluation method of low permeable sandstone pore structure based on nuclear magnetic resonance (NMR) logging. Acta Geophys Sin 59:1543–1552. https://doi.org/10.6038/cjg20160434

Yang XL, Huang F (2011) Collapse mechanism of shallow tunnel based on nonlinear Hoek-Brown failure criterion. Tunn Undergr Sp Technol 26:686–691. https://doi.org/10.1016/j.tust.2011.05.008

Yang XL, Yin JH (2005) Upper bound solution for ultimate bearing capacity with a modified Hoek-Brown failure criterion. Int J Rock Mech Min Sci 42:550–560. https://doi.org/10.1016/j.ijrmms.2005.03.002

Yang XL, Yin JH (2010) Slope equivalent Mohr–Coulomb strength parameters for rock masses satisfying the Hoek–Brown criterion. Rock Mech Rock Eng 43:505–511. https://doi.org/10.1007/s00603-009-0044-2

Yang X, Wang J, Zhu C, He M, Gao Y (2019) Effect of wetting and drying cycles on microstructure of rock based on SEM. Environ Earth Sci 78:183. https://doi.org/10.1007/s12665-019-8191-6

Yao H, Zhang Z, Zhu Z (2011) Uniaxial mechanical properties of sandstone under cyclic of drying and wetting. Adv Mater Res 243–249:2310–2313. https://doi.org/10.4028/www.scientific.net/AMR.243-249.2310

Yao W, Li C, Zhan H, Zhou J-Q, Criss RE, Xiong S, Jiang X (2020) Multiscale study of physical and mechanical properties of sandstone in three Gorges reservoir region subjected to cyclic wetting-drying of Yangtze river water. Rock Mech Rock Eng 53:2215–2231. https://doi.org/10.1007/s00603-019-02037-7

Zhang SJ, Lai YM, Zhang XF, Pu YB, Yu WB (2004) Study on the damage propagation of surrounding rock from a cold-region tunnel under freeze–thaw cycle condition. Tunn Undergr Sp Technol 19:295–302. https://doi.org/10.1016/j.tust.2003.11.011

Zhang Z, Jiang Q, Zhou C, Liu X (2014) Strength and failure characteristics of Jurassic Red-Bed sandstone under cyclic wetting–drying conditions. Geophys J Int 198:1034–1044. https://doi.org/10.1093/gji/ggu181

Zhang J, Deng H, Taheri A, Ke B, Liu C, Yang X (2018) Degradation of physical and mechanical properties of sandstone subjected to freeze-thaw cycles and chemical erosion. Cold Reg Sci Technol 155:37–46. https://doi.org/10.1016/j.coldregions.2018.07.007

Zhang G, Liu EL, Chen SJ, Song BT (2019a) Micromechanical analysis of frozen silty clay-sand mixtures with different sand contents by triaxial compression testing combined with real-time CT scanning. Cold Reg Sci Technol 168:102872. https://doi.org/10.1016/j.coldregions.2019.102872

Zhang J, Deng H, Deng J, Gao R (2019b) Fractal analysis of pore structure development of sandstone: a nuclear magnetic resonance investigation. IEEE Access 7:47282–47293. https://doi.org/10.1109/ACCESS.2019.2909782

Zhao Z, Yang J, Zhang D, Peng H (2017) Effects of wetting and cyclic wetting-drying on tensile strength of sandstone with a low clay mineral content. Rock Mech Rock Eng 50:485–491. https://doi.org/10.1007/s00603-016-1087-9

Zhao YF, Ren S, Jiang DY, Liu R, Wu JX, Jiang X (2018) Influence of wetting-drying cycles on the pore structure and mechanical properties of mudstone from Simian Mountain. Constr Build Mater 191:923–931. https://doi.org/10.1016/j.conbuildmat.2018.10.069

Zheng Y, Chen CX, Liu TT, Song DR, Meng F (2019) Stability analysis of anti-dip bedding rock slopes locally reinforced by rock bolts. Eng Geol 251:228–240. https://doi.org/10.1016/j.enggeo.2019.02.002

Zhou KP, Li JL, Xu YJ, Zhang YM, Yang PQ, Chen LP (2012) Experimental study of NMR characteristics in rock under freezing and thawing cycles, Yanshilixue Yu Gongcheng Xuebao/Chinese. J Rock Mech Eng 31:731–737

Zhou Z, Ma W, Zhang S, Du H, Mu Y, Li G (2016) Multiaxial creep of frozen loess. Mech Mater 95:172–191. https://doi.org/10.1016/j.mechmat.2015.11.020

Zhou ZL, Cai X, Chen L, Cao WZ, Zhao Y, Xiong C (2017) Influence of cyclic wetting and drying on physical and dynamic compressive properties of sandstone. Eng Geol 220:1–12. https://doi.org/10.1016/j.enggeo.2017.01.017